Fibers and Polymers 2016, Vol.17, No.10, 1657-1666
DOI 10.1007/s12221-016-6238-9

ISSN 1229-9197 (print version)
ISSN 1875-0052 (electronic version)

Enhanced Mechanical and Thermal Properties of Hybrid Graphene Nanoplatelets/Multiwall Carbon Nanotubes Reinforced Polyethylene Terephthalate Nanocomposites

I. M. Inuwa, Reza Arjmandi, Akos Noel Ibrahim[1], M. K. Mohamad Haafiz[2], S. L. Wong[3], Khaliq Majeed[4], and Azman Hassan*

Department of Bioprocess and Polymer Engineering, Faculty of Chemical and Energy Engineering, Universiti Teknologi Malaysia, Johor Bahru 81310, Malaysia
[1]*Department of Science Laboratory Technology, School of Science and Technology, Federal Polytechnic Kaura-Namoda 1012, Nigeria*
[2]*School of Industrial Technology, Universiti Sains Malaysia, Penang 11800, Malaysia*
[3]*Department of Chemical Engineering, Faculty of Chemical and Energy Engineering, Universiti Teknologi, Johor Bahru 81310, Malaysia*
[4]*Department of Chemical Engineering, COMSATS Institute of Information Technology, Lahore 54000, Pakistan*
(Received February 15, 2016; Revised August 17, 2016; Accepted August 27, 2016)

Abstract: The effects of graphene nanoplatelets (GNP) and multiwall carbon nanotube (MWCNT) hybrid nanofillers on the mechanical and thermal properties of reinforced polyethylene terephthalate (PET) have been investigated. The nanocomposites were melt blended using the counter rotating twin screw extruder followed by injection molding. Their morphology, mechanical and thermal properties were characterized. Combination of the two nanofillers in composites formulation supplemented each other which resulted in the overall improvement in adhesion between fillers and matrix. The mechanical properties and thermal stability of the hybrid nanocomposites (PET/GNP1.5/MWCNT1.5) were significantly improved compared to PET/GNP3 and PET/MWCNT3 single filer nanocomposites. However, it was observed that GNP was better in improving the mechanical properties but MWCNT resulted in higher thermal stability of Nanocomposite. The transmission electron microscopy (TEM) and field emission scanning electron microscopy (FESEM) revealed uniform dispersion of the hybrid fillers in PET/GNP1.5/MWCNT1.5 nanocomposites while agglomeration was observed at higher filler content. The MWCNT prevented the phenomenal stacking of the GNPs by forming a bridge between adjacent GNP planes resulting in higher dispersion of fillers. This complimentary geometrical structure is responsible for the significant improvement in the thermal stability and mechanical properties of the hybrid nanocomposites.

Keywords: Graphene nanoplatelets, Multiwall carbon nanotubes, Mechanical properties, Thermal properties

Introduction

Engineering thermoplastics such as polyamides and polycarbonates possess superior mechanical and thermal properties, and hence are finding widespread use as structural materials in areas such as the automobile, aircraft or electrical/electronic industries. Consequently, growing demand has led to a hike in prices of these thermoplastics and it is expected that the global revenue for engineering thermoplastics will hit 77 billion dollars by the year 2017 [1]. However, the increasing cost of engineering thermoplastics has motivated researchers both in academia and industry into focusing attention towards finding cheaper alternatives. A commodity thermoplastic such as polyethylene terephthalate (PET) is relatively inexpensive but have lower performance mechanical and thermal properties when compared to engineering thermoplastics. PET is a semi-crystalline commodity thermoplastic with good heat deflection temperature compared to Polypropylene (PP) but poor impact resistance, low melt viscosity and high spinnability. PET has been used in several fields such as food packaging, film technology, beverages containers and textile fibers. Despite its diversity of applications, poor impact properties, low crystallization rate and poor thermal stability of PET polymers limits its functional applications in engineering fields. Therefore, many researchers have focused on improving the mechanical and thermal properties of PET [2,3].

Two highly potent nanofillers that have attracted much attention in the academia and industries are exfoliated graphite nanoplatelets (GNP) and multiwall carbon nanotubes (MWCNT) [4]. Among all the nano additives for polymer nanocomposites, MWCNT are the second most extensively studied nanofillers next only to the silicates layers [4]. MWCNT are graphitic sheets rolled into seamless tubes and have diameters ranging from about a nanometer to tens of nanometers with lengths up to centimeters [5]. MWCNT has received much attention due to their high modulus and effective dispersion in high density polyethylene (HDPE) [6]. Furthermore, MWCNT has been shown to toughen and stiffen amorphous brittle materials such as poly (methyl methacrylate) (PMMA) [7,8] as well as semicrystalline polymers such as HDPE [9]. In addition to the toughening

*Corresponding author: azmanh@cheme.utm.my

and stiffening effects, structural changes have also been reported for semicrystalline polymers such as PP [10].

Single and multiwall carbon nanotubes reinforced PET with improved mechanical properties and thermal stability have also been reported [11,12]. In spite of the various studies, the large scale production of MWCNT reinforced polymer nanocomposites is bedeviled by two constraints; the first is the difficulty to disentangle the tubes for effective dispersion in the polymer matrices which is important for properties enhancement. Overcoming this constraint has been attempted by various techniques such as covalent and non-covalent modification of the nanotubes with reactive moieties which improve the adhesion between nanotubes and polymer matrix [13]. The second disadvantage is the prohibitive cost of production (>200$/kg) for MWCNT [14,15]. All the known processes of carbon nanotube preparation are still prohibitively expensive. However, the problems associated with MWCNTs can be overcome by graphene, the rising star in smart nanomaterials. GNPs are graphitic nanoplatelets which derived from graphite. Their stacked/layered structures, similar to nanoclays, coupled with unique properties such as good thermal conductivity, superior mechanical and physical properties which usually exhibited by carbon nanotubes and also their low-cost (~$10/kg) [14,16] is of great advantage to GNPs. GNPs are characterized by exceptionally high specific surface area and two-dimensional sheet geometry that promote better adhesion with the polymer matrix. Recently, researchers have focused their attention on GNP reinforced polymer nanocomposites [17-19]. Despite these advantages, however, GNP also has the problem of dispersibility in polymer matrix due the $\pi \rightarrow \pi$ attraction and restacking phenomena between graphene planes and it has been an impediment to achieving optimum filler exfoliation and dispersion [20,21].

The need for high performance polymer nanocomposites with excellent mechanical and thermal properties has led to the development of hybrid polymer nanocomposites with multi-type fillers. Hybrid carbon fillers have been used to develop hybrid composites and nanocomposites [22,23]. Hybrid GNP/MWCNT nanocomposites have been reported to have the potential of enhancing the transport properties (e.g., thermal conductivity) of polymer nanocomposites [21, 24-27]. In the investigation of the synergy of GNP/MWCNT hybrid nanofillers on the mechanical properties of epoxy nanocomposites, Li *et al.* [28] recorded a marginal improvement in the flexural properties. Al-Saleh has recently reported a synergy between GNP and MWCNT in PP based composites where the improvements in mechanical properties were attributed to the bridging of the distance between GNP particles by MWCNT particles [29]. In terms of thermal stability recent reports have shown a remarkable improvement of thermal stabilities of polymer composites in the presence of GNP [30,31] or MWCNT [23] or a combination of the two [32]. Although the properties of PET/GNP [33] and PET/MWCNT nanocomposites [11] have been reported individually in the literature, no study is reported on the effects of combination GNPs and MWCNT hybrid fillers on the properties PET prepared via melt blending. The three commonly used methods for the fabrication of nanocomposites are the solution method [34,35], *in situ* polymerization [36-38] and melt blending [39,40]. Among the three methods, melt blending is most suitable because most industrial techniques are based on melt blending even though it has an average dispersion of nanofillers. A recent study has indicated an improved dispersion of GNP particles via melt processing of polyamide 6 [16].

The goal of this study is to exploit the high specific surface area of MWCNT combined with the platelet geometry of GNPs to enhance the properties of PET based hybrid nanocomposites unattainable by the single fillers. In the current study, the effects of hybrid GNP/MWCNT on the mechanical, thermal and morphological properties of PET nanocomposites prepared using melt blending technique were investigated.

Experimental

Materials

Graphene nanoplatelets powders (GNPs) of M grade (99.5 % carbon) of average diameter 5 μm and average thickness of less than 10 nm were purchased from XG Sciences Inc. (East Lansing, MI, USA) and used as received. MWCNTs (Length <50 μm, Diameter <5 nm) were supplied by S.A. Nanocyl (Belgium), grade Nanocyl NC 7000, with 90 % purity and used as received. PET (M100 grade) was obtained from Espet Extrusion Sdn Bhd (Malaysia) with intrinsic viscosity of 0.82 g/d*l*.

Characterization of Filler Properties

A morphological study of GNP and MWCNT was carried out using a transition electron microscope (JEOL JEM-2100 microscope (Tokyo, Japan), operating voltage of 200 kV). The Brunauer, Emmett and Teller (BET) specific surface area of GNP powder and MWCNT were measured by isotherm nitrogen adsorption at 77 K using Micrometrics Gemini V Surface Area Analyzer. The sample was degassed at 623 K under atmospheric pressure for 4 h prior to the BET test. The BET specific area of the sample was calculated using equation (1).

$$S = \frac{V_m N a}{22400 m} \quad (1)$$

V_m: value calculated as 1/(slope+intercept) in the graph of $1/[Va(Po/P)-1]$ against P/Po

N: Avogadro constant (6.022×10^{23} mol^{-1})

a: Effective cross-sectional area of one adsorbate molecule, in square metres (0.162 nm^2 for nitrogen and 0.195 nm^2 for krypton)

m: Mass of test powder, in grams
22400: Volume occupied by 1 mole of the adsorbate gas at STP allowing for minor departures from the ideal, in millilitres

Preparation of Nanocomposites

The PET pellets were dried in a vacuum oven for 24 hours at 120 °C to eliminate moisture which can cause hydrolytic degradation under high temperature. The PET, GNP and MWCNT were then mixed mechanically at room temperature under agitation to disperse the agglomerates. The mixture was then melt blended in a counter rotating twin screw extruder (Brabender Plasticoder, PL 2000) according to Table 1 formulations. This study was designed at a constant filler content of 3 % in all formulations except for 4.5 % which was aimed finding the effect of higher filler loading. The temperature setting from the hopper to the die were 265/275/280/285 °C and the screw speed was 60 rpm. The extruded composites were pelletized and then dried at 120 °C for 12 hours before injection to fabricate standard tensile and flexural test samples using a JSW (Muraron, Japan) model NIOOB II injection-moulding machine. The barrel temperatures were in the range of 250-275 °C. All test specimens were left under ambient conditions in drying desiccators for at least 24 h prior to testing.

Testing and Characterization

Tensile and Flexural Properties

The tensile tests were carried out according to ASTM D638 using Instron 5567 universal testing equipment (Bucks, UK) under ambient conditions at crosshead speed of 50 mm/min. The flexural tests were performed according to ASTM D790 using the Instron 5567 machine under ambient conditions at crosshead speed of 3 mm/min and span distance of 100mm. Five samples of each formulation were tested and the average values were reported.

Thermal Stability

In other to examine the thermal degradation behavior of the samples, thermogravimetric analysis (TGA) was performed using the Perkin Elmer TGA 7 instrument at a heating rate of 10 °C/min under nitrogen atmosphere from 30-600 °C.

Morphological Characterization

Dispersion of the graphite nanoplatelets was observed using field emission scanning electron microscopy (FESEM), transition electron microscopy (TEM). FESEM micrographs of fractured surfaces of the neat PET and nanocomposites were obtained using a Hitachi S-4800. The neat PET and the nanocomposites were gold coated using a Balzers Union MED 010 coater. For TEM analysis, a thin section (thickness of 70 nm) was used for transmission imaging. Samples were microtomed using Reichert Jung Ultracut E microtome. Transmission micrographs were collected using a JEOL JEM-2100 microscope, with an operating voltage of 200 kV.

Chemical Structure Analysis

Fourier transform infrared spectroscopy (FTIR) was used to investigate the nature of the interaction between the various components in the PET/GNP/MWCNT hybrid nanocomposites. The FTIR was performed using a Perkin Elmer 1600 infrared spectrometer. The FTIR spectra were recorded using a Nicolet AVATAR 360 at 16 scans with a resolution of 4 cm^{-1} and wave number range of 370 to 4000 cm^{-1}. The positions of significant transmittance peaks were determined using the "find peak tool" provided by the Nicolet OMNIC 5.01 software.

Table 1. Sample formulations of PET nanocomposites

Sample designation	PET (wt.%)	GNP (wt.%)	MWCNT (wt.%)
PET	100	0	0
PET/GNP3	97	3	0
PET/MWCNT3	97	0	3
PET/GNP1.5/MWCNT1.5	97	1.5	1.5
PET/GNP4.5/MWCNT4.5	91	4.5	4.5

Results and Discussion

Characterization of Fillers

TEM micrographs of GNP and MWCNT are given in Figure 1. It can be seen in Figure 1(a) that GNP appeared as flat sheets which are stacked on each other due the π-π and Van der Waals attraction. According to manufacturers each GNP particle consist of short stacks containing 5-6 graphene layers each. These are then dispersed in the polymer matrix during melt blending as a result of the high temperature and mechanical shear. Figure 1(b) reveals that MWCNT has a long tube-like structure with the average outer diameter of approximately 5 nm as reported by the manufacturers. Obviously the long tubular structure of MWCNT can be seen entangled with each other owing to extremely high aspect ratio and high flexibility of the tubes. MWCNTs are highly entangled and tend to agglomerate into bundles making them difficult to individually disperse into the polymer matrix. Table 2 presents the specific surface area of the fillers obtained from the nitrogen adsorption method (BET). According to the BET analysis, the MWCNT has a specific surface area of 303 m^2/g almost two times that of the GNP which is 158 m^2/g. The formation and dispersion of nanofillers is a function of specific surface area. All other things being equal the dispersion would be better with higher specific surface area nanofillers. However, taking into consideration nanofiller particle shape and agglomeration tendency, surface area may not have controlling effect on nanocomposites formation.

Tensile and Flexural Properties

Table 3 shows the flexural and tensile properties of neat

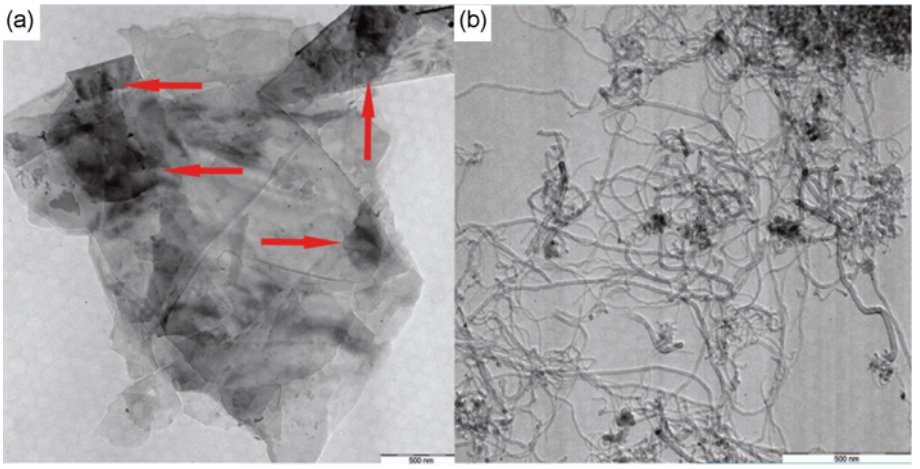

Figure 1. TEM micrographs of (a) GNP and (b) MWCNT powders.

Table 2. BET Surface area of GNP and MWCNT fillers

Filler	Surface area (m^2/g)
GNP	158
MWCNT	303

PET and its nanocomposites. The flexural and tensile moduli of the PET/GNP and PET/MWCNT single filler nanocomposites and PET/GNP/MWCNT hybrid nanocomposites were higher than those of the neat PET. This was attributed to the stiffness and reinforcing effects of the nanofillers in the matrix. Previous studies have shown that the modulus of fibers or particulate reinforced composites mainly depend on the moduli and volume fractions of the composites composition [2,41]. Therefore, since GNP and MWCNT possess very high moduli, it implies that the tensile and flexural moduli of the nanocomposites would be higher than the neat PET. In general, however, the flexural properties are higher than the tensile properties. The slight difference in the magnitude of tensile and flexural moduli between PET/GNP3 and PET/MWCNT3 nanocomposites is attributed to the differences in deformation mode during test (three-point bending in flexural testing vs. failure under extension in tensile), geometry and dimensions of the samples (flex bars for flexural vs. dumb-bell shape samples for tensile) [42]. It also could be due to the differences in stiffness between the layered structure of GNP and flexible, entangled nanotubes. This results in better dispersion and adhesion of the layered GNP to the polymer matrix as compared to the nanotubes. This may explain why the flexural strength of PET/MWCNT3 nanocomposite (77.5 MPa) is lower than the flexural strength of PET/GNP3 nanocomposite (78.3 MPa). Earlier reports have also shown that in addition to strength and volume fraction of the filler, the strength of nanocomposites is controlled by other factors such as polymer-filler interface adhesion, quality of dispersion, the aspect ratio of the filler, specific surface area and orientation [28].

The tensile strengths of PET/GNP3 and PET/MWCNT3 nanocomposites improved significantly as compared to the neat PET in accord with the flexural strength. The improvement was attributed to better dispersion of GNP due to its platelet geometry as compared to the nanotubes. The composites exhibited a decrease in percent elongation at break. This is a typical characteristic of reinforced nanocomposites. The decrease in elongation at break is attributed to the restriction in the polymer chain mobility caused by the rigid filler particles [25,43]. For the hybrid filled nanocomposites, the flexural strength and modulus for PET/GNP1.5/MWCNT1.5 hybrid nanocomposite slightly increased as compared to the single fillers. This is the synergistic effect of GNPs and MWCNTs on flexural strength and modulus of the nanocomposites. Chatterjee *et al.* [44] reported that for epoxy composites the hybrid samples exhibited synergistic effects especially for the flexural modulus where the 9MWCNT:1GNP and 5MWCNT:1GNP proved to be more effective than single filler systems.

The tensile strength and Young's modulus of the hybrid nanocomposites (PET/GNP1.5/MWCNT 1.5) showed imprvemenot compared to the single filler nanocomposites (PET/GNP3, PET/MWCNT3). This was attributed to the homogenous dispersion and interaction between the GNPs and MWCNT in the hybrid system. Zhang *et al.* [45] reported the tensile strength and Young's modulus of PVA nanocomposites filled with only 0.6 wt.% G-MWCNT hybrids are significantly improved by about 77 and 65 %, respectively. Barbosa *et al.* [2] observed improvement of tensile properties of hybrid glass fibers/nanoclays reinforced PET with 1 % nanoclays and 20 % glass fibers. Multiphase composites at high concentration of fillers may also develop structural flaws such as stress concentration which can affect the tensile properties of the material. To investigate the effect of concentration of the hybrid nanofillers on the

Table 3. Flexural and tensile properties of neat PET and PET nanocomposites

Sample name	Flexural strength (MPa)	Flexural modulus (GPa)	Tensile strength (MPa)	Young's modulus (GPa)	Elongation at break (%)
PET	75.9±21.5	2.7±0.2	32.1±11.4	1.1±0.1	3.9±1.0
PET/GNP3	78.3±6.9	3.3±0.2	51.6±3.9	2.8±0.1	2.6±0.3
PET/MWCNT3	77.5±7.5	3.0±0.1	44.4±7.9	2.5±0.4	2.5±0.5
PET/GNP1.5/MWCNT1.5	84.5±13.1	3.4±0.2	57.4±9.4	2.3±0.6	3.0±1.2
PET/GNP4.5/MWCNT4.5	75.7±16.0	3.5±0.3	44.0±7.8	2.7±0.7	2.5±0.8

mechanical properties of the PET composites, equal ratio of 4.5 wt.% GNP and MWCNT was further studied. As shown in Table 3, no significant improvement in the tensile and flexural properties of PET/GNP4.5/MWCNT4.5 hybrid nanocomposite was observed. This was attributed to agglomeration of the GNPs and MWCNTs at higher filler loading. The agglomeration in the composites is due to the Van der Waals forces in MWCNT and strong π→π interaction in the graphene planes which prevents them from dispersing in the matrix. This observation is consistent with other studies which reported similar findings on GNP/MWCNT hybrid fillers in epoxy composites [44]. The attractive forces in GNP and MWCNT became less effective for the PET/GNP1.5/MWCNT1.5 hybrid nanocomposite due to the interaction between GNP and MWCNT thereby helped in the dispersion of the fillers and improving adhesion with the matrix.

Thermal Stability

Thermogravimetric analysis (TGA) was used to study the thermal stability of the neat PET and PET nanocomposites. A typical TGA curve for thermal degradability shows a sample subjected to heat will slowly suffer weight loss; the weight will then drop sharply over a narrow range before turning back to zero slope as the reactant is exhausted. At 300-500 °C, polymer matrices decompose, releasing heat and toxic volatiles. Decomposition of burning polymers includes the production of combustible gases, non-combustible gases, liquids, solids (usually char), and entrained solid particles. Figure 2(a) and (b) shows the thermogravimetric analysis (TGA) and its derivative DTG respectively for the neat PET and PET/GNP/MWCNT hybrid nanocomposites while their corresponding data is shown in Table 4. The neat PET and all the nanocomposites show a single step decomposition process. The similar decomposition patterns indicate that GNPs and MWCNTs do not affect the basic degradation pathways of PET which was an indication of absence of structural changes in the matrix due to presence of the fillers. The addition of GNP, MWCNT and GNP/MWCNT hybrid fillers improved the thermal stability of the nanocomposites compared to neat PET as shown in Table 4. The TGA onset temperature, T_{onset} is the temperature at which weight loss begins. Increase in T_{onset} is an indication of higher thermal stability for the nanocomposites.

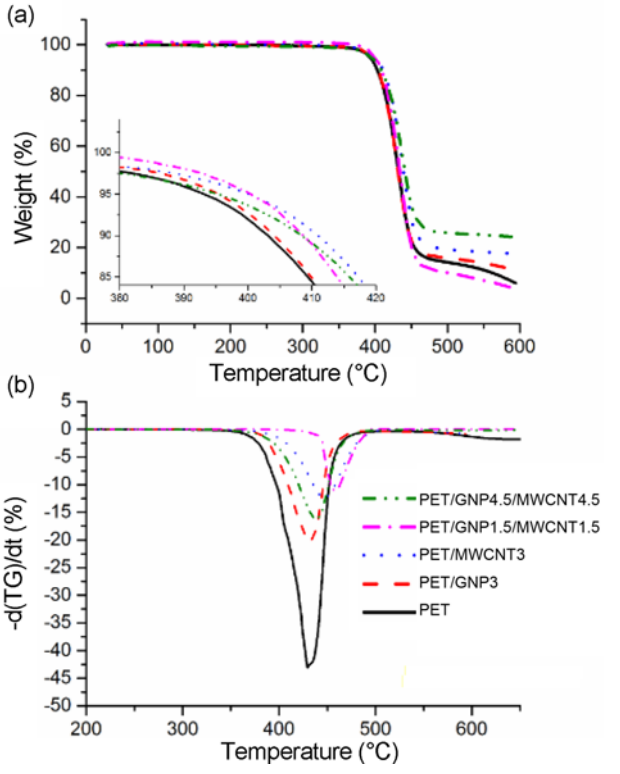

Figure 2. (a) TGA and (b) DTG thermograms of neat PET, PET/GNP3 nanocomposite, PET/MWCNT3 nanocomposite and PET/GNP/MWCNT hybrid nanocomposites.

Table 4. TGA and DTG data under nitrogen atmosphere at 10 °C/min

Designation	T_{onset} (°C)	T_{max}	Char residue (%)
PET	380.0	425.9	6.1
PET/GNP3	388.7	432.6	11.1
PET/MWCNT3	391.7	452.3	17.5
PET/GNP1.5/MWCNT1.5	393.4	468.4	23.8
PET/GNP4.5/MWCNT4.5	391.0	439.6	24.1

The T_{onset} for the neat PET was 380 °C. For PET/GNP3 and PET/MWCNT3 nanocomposites, the T_{onset} increased to 388.7 and 391.7 °C respectively. It can be seen that MWCNT

yielded a more thermally stable nanocomposites compared to the GNPs. The improved thermal stability toward higher temperatures were due to the barrier effect of the incorporated nanoparticles. The higher thermally stable GNP and MWCNT particles hinder the diffusion of the gaseous degradation products of the composites. This finding is consistent with earlier reports [12,46]. Also, T_{onset} of 393.4 °C for PET/GNP1.5/MWCNT1.5 hybrid nanocomposite is slightly higher than the T_{onset} of PET/GNP3 (388.7 °C) and PET/MWCNT3 nanocomposites (391.7 °C). This indicates the synergy between the GNP and MWCNT fillers. The synergy between GNP and MWCNT in the thermal stability of polyetherimide nanocomposites have been reported [21]. The synergistic effect is however more pronounced at the peak decomposition temperature, T_{max}. The T_{max} of 468.4 °C for PET/GNP1.5/MWCNT1.5 hybrid nanocomposites is significantly higher than that of PET/GNP3 (432.6 °C) and PET/MWCNT3 nanocomposites (452.3 °C). Pradhan and Bratati [32] made a similar observation in their studies on the synergistic effect of three-dimensional multi-walled carbon nanotube-graphene nanofillers in enhancing the mechanical and thermal properties of high-performance silicone rubber. The difference in the T_{max} between PET/GNP3 and PET/MWCNT3 nanocomposites is attributed to the differences in the dispersion situation and thermal stability of GNPs and MWCNT. Similar observation was made by Du *et al.* [47] when they compared MWCNT/HDPE nanocomposites and GNP/HDPE nanocomposites. It is interesting to note that at higher concentration of the hybrid fillers (GNP4.5/MWCNT4.5), the T_{onset} and T_{max} of PET/GNP4.5/MWCNT4.5 is lower than that of PET/GNP1.5/MWCNT1.5 hybrid nanocomposites. This is attributed to the agglomeration of the nanofillers as a result of increase in interaction in the composites with high filler concentration. The increase in the char residue level is a reflection of the improved thermal stability of GNP and MWCNT filled

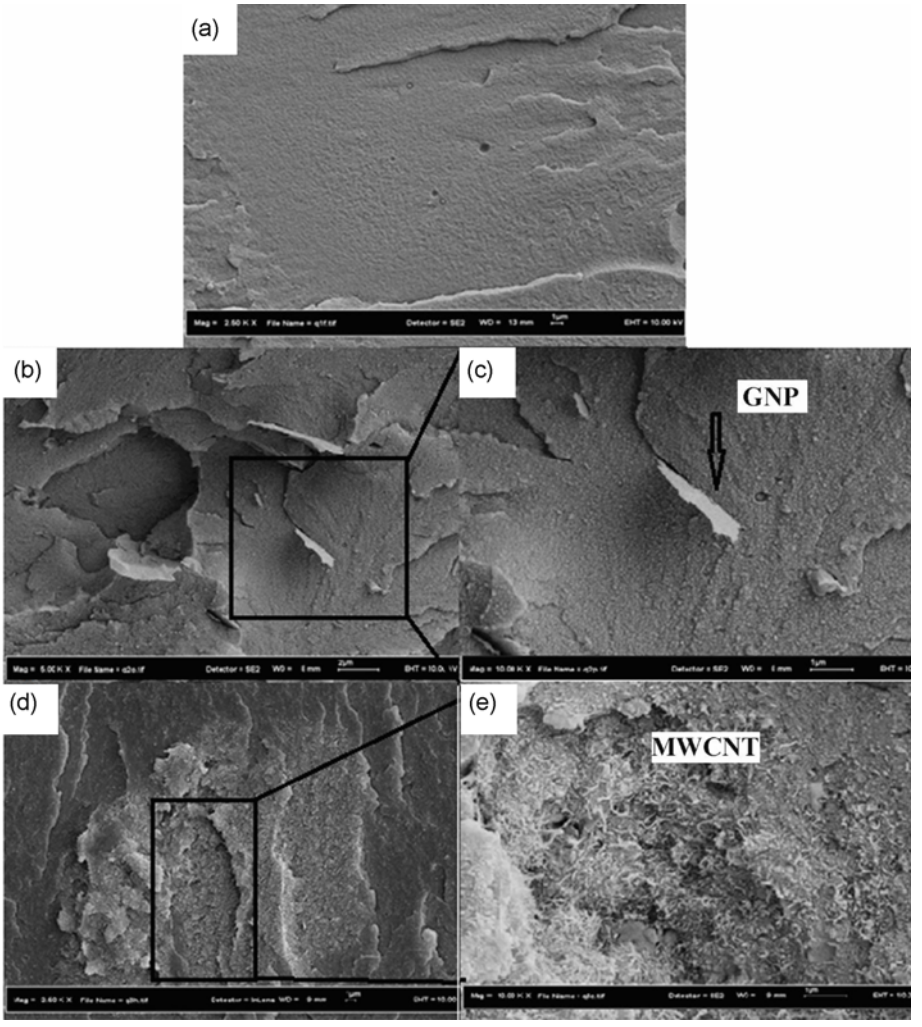

Figure 3. FESEM images showing the morphology of fractured surface of the PET nanocomposites; (a) neat PET, (b) PET/GNP3 nanocomposite, (c) magnified section of (b), (d) PET/MWCNT3 nanocomposite and (e) magnified section of (d).

polymer nanocomposites as shown in Table 4. The nanocomposites have higher char content as compared to the neat PET. The char values increased with increasing concentration of the nanofillers in an additive manner.

Morphological Characterization

The uniform dispersion of nanoparticles in polymer matrices is important in the fabrication of nanocomposites. Van der Waals forces and differences in polymer/nanoparticle surface energies often cause the particles to have greater affinity towards each other than the polymer matrix they are being incorporated into. The high affinity between the nanoparticles leads to the problem of agglomeration [31, 48]. Figure 3 shows the FESEM surface morphology of GNP, MWCNT and GNP/MWCNT hybrid reinforcements in the PET matrix. Figure 3(a) is the FESEM micrograph of neat PET. The surface smoothness and homogeneity of the neat PET can be recognized as freeze-fractured surface of neat PET in the absence of fillers, which can be compared to the rough surfaces and contours of the GNP and MWCNT filled nanocomposites.

Figure 3(b) and (c) show the FESEM micrograph of PET nanocomposites containing 3 wt.% GNP filler at low and high magnification. The GNPs can be seen to be homogeneously dispersed in the PET matrix with no agglomeration. The good dispersion of the graphene sheets is attributed to the two-dimensional planer geometry of GNP which resembles the layered clay-like structure and promoted the dispersion in the matrix. In Figure 3(c) the individual GNP particles can be seen embedded in the matrix with one end protruding out of the plane of the fractured surface. Figure 3(d) and (e) show the dispersion of MWCNTs in the PET matrix. Figure 3(e) shows the clusters of MWCNT on the surface of the fractured nanocomposites. Nonetheless the GNPs and MWCNTs at 3 wt.% loading were generally observed to be dispersed in the PET matrix. This implies some level of adhesion that led to effective stress transfer from the matrix to the fillers which led to improvement in the tensile and flexural properties. This effect is reflected in the improved mechanical properties of the PET/GNP3 and PET/MWCNT3 nanocomposites. However, the dispersion in the hybrid nanocomposites is depicted in the FESEM and TEM micrographs shown in Figure 4 and 5. Figure 4(a) (magnified in Figure 4(b)) and 4(c) (magnified in Figure 4(d)) show the interaction between the GNPs and MWCNT in PET matrix which is occasioned by Van der Waals attractive forces. Figure 5(a) shows the TEM micrograph of the hybrid nanocomposites with GNP1.5/MWCNT1.5. Close examination revealed that both the GNPs and MWCNT are well dispersed throughout the matrix as pointed by the arrows. The large planer GNPs may provide a platform to assemble the ends of MWCNTs through π-π interactions. On the other hand, MWCNTs act to prevent the restacking of GNPs as indicated. The uniform dispersion of MWCNT ensured that GNP restacking is prevented. This would account for observed improvement in the tensile and flexural properties and the thermal stability of the hybrid nanocomposites. Schematic representation of this interaction

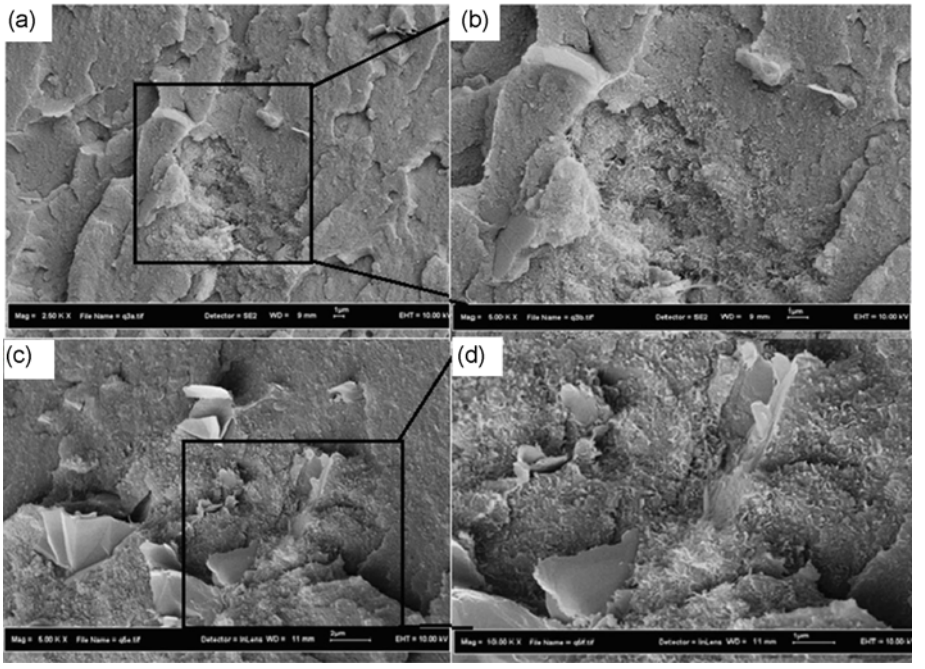

Figure 4. FESEM images showing the morphology of fracture surface of the PET nanocomposites; (a) PET/GNP1.5/MWCNT 1.5 hybrid nanocomposite, (b) magnified section of (a), (c) PET/GNP4.5/MWCNT4.5 hybrid nanocomposite and (d) magnified section of (c).

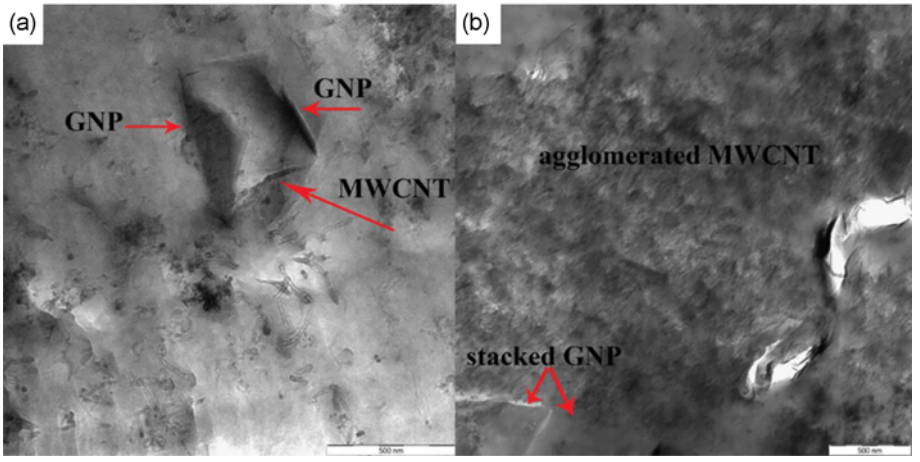

Figure 5. TEM micrograph of (a) PET/GNP1.5/MWCNT1.5 hybrid nanocomposite showing the interaction of GNPs and MWCNTs and (b) agglomeration of MWCNT and GNP at higher concentration.

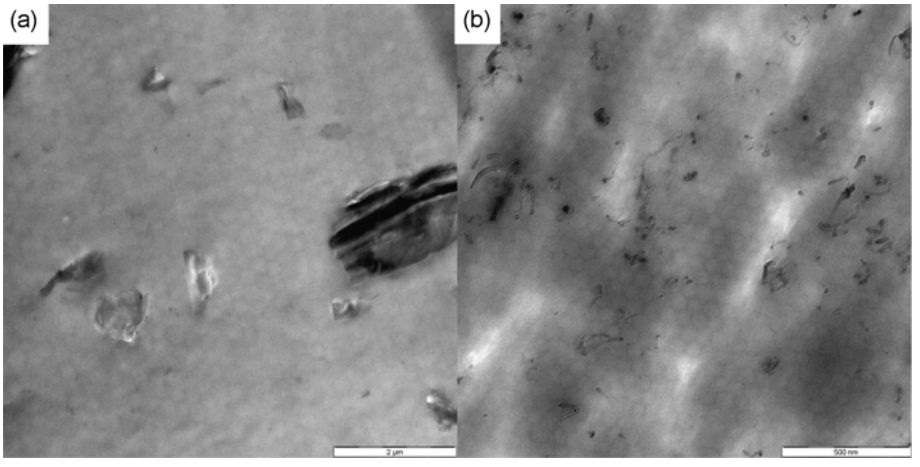

Figure 6. TEM images of (a) PET/GNP3 and (b) PET/MWCNT3 nanocomposites.

is depicted in Figure 6. In Figure 5(b), the effect of higher concentration can be seen where both the MWCNT and the GNPs started to agglomerate which led to the drop in the mechanical and thermal properties at 4.5 phr for the PET/GNP/MWCNT hybrid nanocomposites.

The incorporation of MWCNTs greatly influences the dispersion of GNPs in the polymer. This is because the inclusion of MWCNT within the GNP planes prevented the restacking of graphene sheets. This has demonstrated the synergy between GNPs and MWCNTs in the PET matrix resulting in the improvement in the properties of the polymer [49,50].

Figure 6(a) shows the TEM image of PET/GNP3 nanocomposite, it can be seen that GNP fillers are uniformly distributed and is indicative of the improvement in the tensile properties and modulus as discussed earlier. Similar observation was made with PET/MWCNT3 nanocomposite where nanotube was shown to be well dispersed in the matrix.

FTIR Spectroscopy

Figure 7 shows the FTIR transmission spectra of neat PET, PET/GNP1.5/MWCNT1.5 hybrid nanocomposite, PET/MWCNT3 and PET/GNP3 nanocomposites, and MWCNT and GNP powders. For the purpose of comparison, the spectra are shifted along the y-axis. The observed bands for neat PET are similar to those presented in Table 5 [51-56]. The bands at 1723 cm^{-1}, 1410 cm^{-1} and 1342 cm^{-1} corresponds to the ester carbonyl stretching [51], para substituted benzene ring [57], and the ethylene group (wagging) respectively. The band around 1261 cm^{-1} is mainly due to vibrations of the ester group [58]. The peak at 725 cm^{-1} is assigned to C-C (ring) bending and C-H (ring) out of plane [55]. The peak at 3440 cm^{-1} is assigned to the OH intermolecular hydrogen bonding. No visible peaks were observed in the spectrum of GNP powder which indicates the absence of any functional group [59,60].

The very weak band at around 3444 cm^{-1} for MWCNT is due to the stretching vibrations of isolated surface -OH

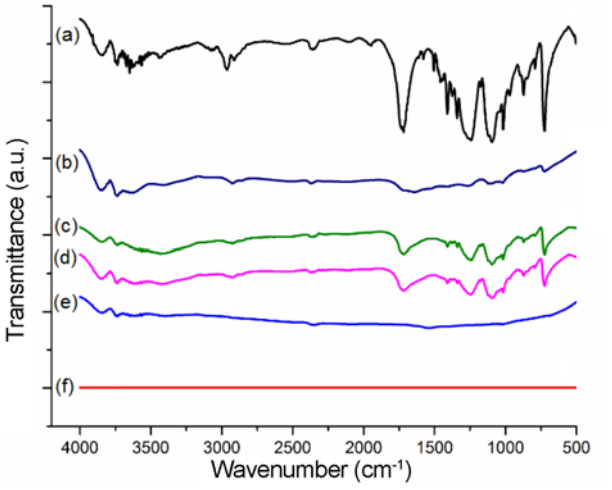

Figure 7. FTIR spectra of (a) neat PET, (b) PET/GNP1.5/MWCNT1.5 hybrid nanocomposite, (c) PET/MWCNT3 nanocomposite, (d) PET/GNP3 nanocomposite, (e) MWCNT powder, and (f) GNP powder.

Table 5. Major peak positions FTIR band wavenumbers (cm^{-1}) and the corresponding assignments for neat PET

Wave number (cm^{-1})	Assignment	Reference
2970	C-H vibration, C-H stretching	[34,37]
1723	C=O stretching	[31,32,33]
1261	Ester group (Vibration)	[31,36]
1110	Para substituted benzene ring, C-O-C asymmetric stretching	[33,37]
725	C-C (ring) bending, C-H out of plane	[31,32,37]
1410	C-C ring stretching	[32]
1342	CH_2 wagging	[32,33]
872	Aromatic ring	[37]
3440	-OH intermolecular hydrogen bonding	[37]

moieties and/or -OH in carboxyl groups and in absorbed water [61]. For PET/GNP1.5/MWCNT1.5 hybrid nanocomposites, PET/GNP3 and PET/MWCNT3 nanocomposites, no significant changes in peak positions were observed as compared to neat PET. This implies the absence of any significant chemical interaction between GNPs, MWCNTs and neat PET matrix. In view of the above, the change in properties exhibited by the nanocomposites is only due to physical interactions between the GNPs, MWCNT and the PET matrix. This indicated that the interaction between the carbon nanoparticles is through the Van der Waals forces and π-π attractions as indicated earlier.

Conclusion

PET/GNP and PET/MWCNT nanocomposites, and PET/GNP/MWCNT hybrid nanocomposites were prepared by melt extrusion technique and the effects of filler content on flexural, tensile and thermal properties were investigated. The tensile and flexural properties were improved with addition of GNP and MWCNT. However, improvement of mechanical properties due to GNP was higher than the MWCNT. Synergy was observed with 1.5 wt.% each of GNP and MWCNT in the PET matrix. However, a more pronounced synergy is manifested as the GNP/MWCNT hybrid fillers improved the thermal stability of the composite significantly when compared to the individual composites of GNP and MWCNT. It was observed that the improvement in thermal stability with MWCNT was higher than the GNPs. Furthermore, at high hybrid filler concentration (9 wt.%), the mechanical and thermal properties of the composites dropped due to filler agglomeration. The morphology by FESEM and TEM showed uniform dispersion of the hybrid fillers at 1.5 wt.% GNP and 1.5 wt.% MWCNT content due to the interaction between MWCNT and GNPs. The FTIR revealed that only physical interactions existed between the PET matrix, MWCNT and GNP fillers as no significant changes in the peak position was observed. The improved nanocomposites developed will have potential application in the automobile industries thereby expanding the area of applications of PET beyond its traditional use in the fibers and packaging industries.

Acknowledgement

The authors wish to acknowledge the Universiti Teknologi Malaysia (UTM), Ministry of Higher Education Malaysia (MOHE) and Research University Grant 10H94, sub-code: Q.J130000.2544.10H94 for financial support.

References

1. I. M. Inuwa, A. Hassan, and S. A. Samsudin, *Malays. J. Anal. Sci.*, **18**, 466 (2014).
2. C. N. Barbosa, F. Goncalves, and J. C. Viana, *Adv. Polym. Technol.*, **33** (2014).
3. Q. L. Li, X. L. Wang, D. Y. Wang, Y. Z. Wang, X. N. Feng, and G. H. Zheng, *J. Appl. Polym. Sci.*, **122**, 342 (2011).
4. J. Wu, K. Yu, K. Qian, and Y. Jia, *Fiber. Polym.*, **16**, 1540 (2015).
5. P. C. Ma, N. A. Siddiqui, G. Marom, and J. K. Kim, *Compos. Pt. A-Appl. Sci. Manuf.*, **41**, 1345 (2010).
6. M. A. Mohsin, A. Arsad, S. K. Gulrez, Z. Muhamad, H. Fouad, and O. Y. Alothman, *Fiber. Polym.*, **16**, 129 (2015).
7. G. B. Huang, S. Q. Chen, S. W. Tang, and J. R. Gao, *Mater. Chem. Phys.*, **135**, 938 (2012).
8. X. Wen, Y. J. Wang, J. Gong, J. Liu, N. N. Tian, Y. H. Wang, Z. W. Jiang, J. Qiu, and T. Tang, *Polym. Degrad. Stabil.*, **97**, 793 (2012).
9. W. Z. Tang, M. H. Santare, and S. G. Advani, *Carbon*, **41**,

2779 (2003).
10. E. M. Sullivan, Y. J. Oh, R. A. Gerhardt, B. Wang, and K. Kalaitzidou, *J. Polym. Res.*, **21**, 1 (2014).
11. K. Anand, U. Agarwal, and R. Joseph, *J. Appl. Polym. Sci.*, **104**, 3090 (2007).
12. J. Y. Kim, H. S. Park, and S. H. Kim, *J. Appl. Polym. Sci.*, **103**, 1450 (2007).
13. F. C. Chiu and Y. J. Chen, *Compos. Pt. A-Appl. Sci. Manuf.*, **68**, 62 (2015).
14. S. P. Liu, *J. Ind. Eng. Chem.*, **20**, 2401 (2014).
15. J. Huang and D. Rodrigue, *Mater. Des.*, **65**, 974 (2015).
16. B. Mayoral, E. Harkin-Jones, P. N. Khanam, M. A. AlMaadeed, M. Ouederni, A. R. Hamilton, and D. Sun, *Rsc. Adv.*, **5**, 52395 (2015).
17. X. Jiang and L. T. Drzal, *Polym. Compos.*, **31**, 1091 (2010).
18. S.-H. Hwang, B.-J. Kim, J.-B. Baek, H. S. Shin, I.-J. Bae, S.-Y. Lee, and Y.-B. Park, *Compos. Pt. B-Eng.*, **100**, 220 (2016).
19. L. Ji, P. Meduri, V. Agubra, X. Xiao, and M. Alcoutlabi, *Adv. Energy Mater.*, **6**, 1502159 (2016).
20. C. A. Crock, A. R. Rogensues, W. Q. Shan, and V. V. Tarabara, *Water Res.*, **47**, 3984 (2013).
21. S. Kumar, L. L. Sun, S. Caceres, B. Li, W. Wood, A. Perugini, R. G. Maguire, and W. H. Zhong, *Nanotechnology*, **21**, 105702 (2010).
22. M. H. Al-Saleh and W. H. Saadeh, *Mater Des.*, **52**, 1071 (2013).
23. M. L. Manchado, L. Valentini, J. Biagiotti, and J. Kenny, *Carbon*, **43**, 1499 (2005).
24. M. Lewin, E. M. Pearce, K. Levon, A. Mey-Marom, M. Zammarano, C. A. Wilkie, and B. N. Jang, *Polym. Adv. Technol.*, **17**, 226 (2006).
25. I. M. Inuwa, A. Hassan, S. A. Samsudin, M. K. M. Haafiz, M. Jawaid, K. Majeed, and N. C. A. Razak, *J. Appl. Polym. Sci.*, **131**, 40582 (2014).
26. M. Safdari and M. S. Al-Haik, *Carbon*, **64**, 111 (2013).
27. M. Chen, T. Tao, L. Zhang, W. Gao, and C. Li, *Chem. Commun.*, **49**, 1612 (2013).
28. J. Li, P. S. Wong, and J. K. Kim, *Mat. Sci. Eng. A-Struct.*, **483-484**, 660 (2008).
29. M. H. Al-Saleh, *Synth. Met.*, **209**, 41 (2015).
30. F. He and J. Fan, *Proc. MRS*, **1129**, 11 (2011).
31. S. Kim, I. Do, and L. T. Drzal, *Polym. Compos.*, **31**, 755 (2010).
32. B. Pradhan and S. K. Srivastava, *Polym. Int.*, **63**, 1219 (2014).
33. H. B. Zhang, W. G. Zheng, Q. Yan, Y. Yang, J. W. Wang, Z. H. Lu, G. Y. Ji, and Z. Z. Yu, *Polymer*, **51**, 1191 (2010).
34. H. M. Kim, J. K. Lee, and H. S. Lee, *Thin Solid Films*, **519**, 7766 (2011).
35. J. Bian, X. Wei, H. Lin, L. Wang, and Z. Guan, *J. Appl. Polym. Sci.*, **124**, 3547 (2012).
36. V. Alzari, D. Nuvoli, R. Sanna, S. Scognamillo, M. Piccinini, J. M. Kenny, G. Malucelli, and A. Mariani, *J. Mater. Chem.*, **21**, 16544 (2011).
37. S. Mohamadi, N. Sharifi-Sanjani, and A. Foyouhi, *J. Polym. Res.*, **20**, 1 (2013).
38. S. G. Kim, E. A. Lofgren, and S. A. Jabarin, *Adv. Polym. Technol.*, **32** (2013).
39. I. M. Inuwa, A. Hassan, S. A. Samsudin, M. K. M. Haafiz, and M. Jawaid, *Polym. Compos.*, **35**, 2029 (2014).
40. I. M. Inuwa, A. Hassan, D. Y. Wang, S. A. Samsudin, M. K. M. Haafiz, S. L. Wong, and M. Jawaid, *Polym. Degrad. Stabil.*, **110**, 137 (2014).
41. Y. Yoo, H. L. Lee, S. M. Ha, B. K. Jeon, J. C. Won, and S. G. Lee, *Polym. Int.*, **63**, 151 (2014).
42. K. Kalaitzidou, H. Fukushima, H. Miyagawa, and L. T. Drzal, *Polym. Eng. Sci.*, **47**, 1796 (2007).
43. P. Nemes-Incze, Z. Osvath, K. Kamaras, and L. P. Biro, *Carbon*, **46**, 1435 (2008).
44. S. Chatterjee, F. Nafezarefi, N. H. Tai, L. Schlagenhauf, F. A. Nuesch, and B. T. T. Chu, *Carbon*, **50**, 5380 (2012).
45. C. Zhang, S. Huang, W. W. Tjiu, W. Fan, and T. X. Liu, *J. Mater. Chem.*, **22**, 2427 (2012).
46. X. Yi, L. Xu, Y. L. Wang, G. J. Zhong, X. Ji, and Z. M. Li, *Eur. Polym. J.*, **46**, 719 (2010).
47. J. H. Du, L. Zhao, Y. Zeng, L. L. Zhang, F. Li, P. F. Liu, and C. Liu, *Carbon*, **49**, 1094 (2011).
48. E. T. Thostenson, C. Y. Li, and T. W. Chou, *Compos. Sci. Technol.*, **65**, 491 (2005).
49. W. K. Li, A. Dichiara, and J. B. Bai, *Compos. Sci. Technol.*, **74**, 221 (2013).
50. S. Y. Yang, W. N. Lin, Y. L. Huang, H. W. Tien, J. Y. Wang, C. C. M. Ma, S. M. Li, and Y. S. Wang, *Carbon*, **49**, 793 (2011).
51. M. Djebara, J. P. Stoquert, M. Abdesselam, D. Muller, and A. C. Chami, *Nucl. Instrum. Meth. B*, **274**, 70 (2012).
52. C. Sammon, J. Yarwood, and N. Everall, *Polym. Degrad. Stabil.*, **67**, 149 (2000).
53. G. Guclu, T. Yalcinyuva, S. Ozgumu, and M. Orbay, *Thermochim Acta*, **404**, 193 (2003).
54. Z. Y. Zhu, C. L. Liu, Y. M. Sun, J. Liu, Y. H. Tang, Y. F. Jin, and J. L. Du, *Nucl. Instrum. Meth. B*, **191**, 723 (2002).
55. C. C. Tan, I. Ahmad, and M. C. Heng, *Mater. Des.*, **32**, 4493 (2011).
56. K. C. Cole, A. Ajji, and E. Pellerin, *Macromol. Symp.*, **184**, 1 (2002).
57. Z. M. Zhu and M. J. Kelley, *Polymer*, **46**, 8883 (2005).
58. K. C. Cole, A. Ajji, and E. Pellerin, *Macromolecules*, **35**, 770 (2002).
59. Y. Geng, S. J. Wang, and J. K. Kim, *J. Colloid Interface Sci.*, **336**, 592 (2009).
60. J. Cao, Y. Wang, K. Ke, Y. Luo, W. Yang, B. H. Xie, and M. B. Yang, *Polym. Int.*, **61**, 1031 (2012).
61. X. L. Ling, Y. Z. Wei, L. M. Zou, and S. Xu, *Colloid Surf. A-Physicochem. Eng. Asp.*, **421**, 9 (2013).